An integrated approach to highlight biological responses of *Pisum sativum* root to nano-TiO_2 exposure in a biosolid-amended agricultural soil.

Giorgetti L.[1*], Spanò C.[2*], Muccifora S.[3], Bellani L.[1,3], Tassi E.[4], Bottega S.[2], Di Gregorio S.[2], Siracusa G.[2], Sanità di Toppi L.[2], Ruffini Castiglione M.[2]

*Co-first Authors

[1] Institute of Agricultural Biology and Biotechnology, UOS Pisa, CNR, Via Moruzzi 1, 56124 Pisa, Italy

[2] Department of Biology, University of Pisa, Via Ghini 13, 56126 Pisa, Italy

[3] Department of Life Sciences, University of Siena, Via A. Moro 2, 53100 Siena, Italy

[4] Institute of Ecosystem Studies, National Research Council (ISE-CNR), via Moruzzi 1, 56124 Pisa, Italy

Corresponding author:

Monica Ruffini Castiglione, Department of Biology, University of Pisa, Via Ghini 13, 56126 Pisa, Italy. E-mail: monica.ruffini.castiglione@unipi.it

Tel. +390502211317

Abstract

This study focused on crop plant response to a simultaneous exposure to biosolid and TiO_2 at micro- and nano-scale, being biosolid one of the major sink of TiO_2 nanoparticles released into the soil environment. We settled an experimental design as much as possible realistic, at microcosm scale, using the crop *Pisum sativum.* This experimental design supported the hypotheses that the presence of biosolid in the farming soil might influence plant growth and metabolism and that, after TiO_2 spiking, the different dimension and crystal forms of TiO_2 might be otherwise bioavailable and differently interacting with the plant system. To test these hypotheses, we have considered different aspects of the response elicited by TiO_2 and biosolid at cellular and organism level, focusing on the root system, with an integrative approach. In our experimental conditions, the presence of biosolid disturbed plant growth of *P. sativum*, causing cellular damages at root level, probably through mechanisms not only oxidative stress-dependent but also involving altered signalling processes. These disturbances could depend on non-humified compounds and/or on the presence of toxic elements and of nanoparticles in the biosolid-amended soil. The addition of TiO_2 particles in the sludge-amended soil, further altered plant growth and induced oxidative and ultrastructural damages. Although non typical dose-effect response was detected, the most responsiveness treatments were found for the anatase crystal form, alone or mixed with rutile. Based on ultrastructural observations, we could hypothesise that the toxicity level of TiO_2 nanoparticles may depend on the cell ability to isolate nanoparticles in subcellular compartments, avoiding their interaction with organelles and/or metabolic processes.

The results of the present work suggest reflections on the promising practice of soil amendments and on the use of nanomaterials and their safety for food plants and living organisms.

Keywords

Biosolid, cell compartments, oxidative stress, pea, root, titanium dioxide particles.

1. Introduction

Contaminants of emerging concern are increasingly gaining ground in all the ecosystems, due to the unintentional or intentional release into the environment of new molecules/compounds or to a new employment and disposal of complex and potentially polluted matrices (Halden 2015). In this context, the reuse of sludge from wastewater treatment plants (WWTP) in farming soils is recognized as a cost-effective practice to dispose of a byproduct that can be applied to the soil-plant system as a fertilizer, rich in organic matter and nutrients (Lu et al. 2012; EPA 1994). Regulations governing the reuse of biosolid (Bs) in farming applications take several broad forms in different countries, but basically they follow a code of good practice, which foresees specific treatments and maturation aimed to guarantee defined chemical, physical and microbiological standards (EEC 1986; EPA 1993).

On the other hand, due to the uncertainty of its content not thoroughly tested for safety, Bs can result a possible sink of organic and inorganic unknown priority pollutants as well as of not commonly monitored chemicals, such as nanoparticles (NPs) (Brar et al. 2010; Yang et al. 2014).

The nanotechnology revolution and its challenges has been going on for some time, accompanied however by a series of ethical/safety implications related to the release into the environment of new nano-chemical compounds whose effects on ecosystems and living organisms are not yet fully clear and unambiguously interpretable (Maurer-Jones et al. 2013). Besides, NPs behavior is poorly estimated in the different environmental matrices, especially

76 in agricultural soils. In such complex matrices, the bioavailability of the different NPs often is
77 not predictable, due to their tendency to aggregate, to adsorb/precipitate on solid phase, as
78 well as to be coated by organic molecules (Tourinho et al. 2012; Pachapur et al. 2016). In
79 addition, the overall picture of their possible interactions with crop plants and with food
80 chains are not at all clear (Ruffini Castiglione and Cremonini 2009; Remedios et al. 2012;
81 Rico et al. 2011; Tassi et al. 2017). Given that we can not afford to miss the opportunity of
82 exploiting nanotechnologies, it is priority and urgent to dispel these uncertainties, that
83 nowadays remain, about the possible harmful effects of these nanomaterials, otherwise
84 transferred in farming soils, on crop plants and food chains.
85 TiO_2 NPs are among the top five nanomaterials widely used for various applications
86 (Chuankrerkkul and Sangsuk 2008), ranging from food and personal care products (Weir et
87 al. 2012) to specific medical devices coating (Villatte et al. 2015) and drug delivery systems
88 (Bakhshizadeh et al. 2017), from coating pigments production (El-Sherbiny et al. 2014) to
89 their employment in certain farming sectors and in environmental cleanup technologies
90 (Bhawana and Fulekar 2012; Liu 2011). A broad sector of the current body of literature on the
91 environmental impact of NPs is focused on this class of nanomaterials: in recent years, the
92 number of studies on their effects on higher plants is increasing, as well as the different
93 experimental approaches and endpoints considered to evaluate NPs uptake, translocation,
94 accumulation in plant tissues/organs and potential toxicity (Larue et al. 2012; Song et al.
95 2013; Ruffini Castiglione et al. 2014, Ruffini Castiglione et al. 2016; Amini et al. 2017). The
96 researchers' guidance on these issues is also connected to the general awareness and concern
97 that the most used NPs, including TiO_2, may easily and in a short time reach significant
98 environmental concentrations and enter in the food chains through crop plants, thus affecting
99 the whole living organisms (Rico et al. 2011).
100 Most of the works published so far on TiO_2 NPs effects on plants of agronomic interest report

101 data obtained in hydroponics, water suspensions or under any other experimental conditions
102 to monitor the short-term effects, testing high concentrations of TiO_2 (Maurer-Jones et al.
103 2013; Cox et al. 2016), often not realistic, even in the case of accidental pollution (Sun et al.
104 2014). In this context, there are few studies involving the use of agricultural soils as growth
105 substrates for plants along with the application of treatments (Du et al. 2011; Burke et al.
106 2014; Gogos et al. 2016).
107 In this report, we settled an experimental design as much as possible realistic, at microcosm
108 scale, using a biosolid-amended agricultural soil as growth matrix for the crop *Pisum sativum.*
109 We aimed to investigate the effects of TiO_2 in the form of bulk material and in three different
110 nanoparticulate formulations: crystals of anatase, rutile, and a mix of both, all applied at two
111 different concentrations in the range established simulating an environmental contamination,
112 and under long term exposure. This experimental design supports the hypotheses that the
113 presence of Bs in itself may influence plant growth and metabolism and that, after TiO_2
114 spiking, the different dimension and crystal forms of titanium dioxide might be otherwise
115 bioavailable and differently interacting with the plant system. To test our hypotheses, we have
116 chosen to take into account different aspects of the response elicited by TiO_2 and Bs in
117 tissues/organs, at cellular and organism level, focusing on the root system, with an integrative
118 approach.
119
120
121
122 **2. Materials and Methods**
123
124 *2.1 Growth substrates*
125 The farming soil (C1) was collected at CiRAA - Agri-Environmental Research Center 'Enrico

126 Avanzi' from University of Pisa, Italy. The soil was air-dried, sieved (0-2 mm) and
127 homogenized before its analysis and use as growth substrate. C1 soil was characterized by a
128 sandy texture (93.3% of sand, 4.6% of silt and 2.1% of clay) with a pH near the neutrality
129 (7.7), low organic matter content (OM, 1.1%), medium value of cation exchange capacity
130 (CEC, 15.5 $cmol^{(+)}$ kg^{-1}) and electrical conductivity (EC) of 0.80 mS cm^{-1}.
131 Bs was obtained from a small WWTP in Pisa (Italy) as a dewatered sludge qualified for its
132 use in an agricultural soil. Bs was further characterized by having a solid residue (at 105°C)
133 of 18%, pH of 6.9, high OM (57.3%), EC of 11.5 mS cm^{-1} and total concentration of Ti of
134 699 ± 105 mg kg-1 (dw basis). Titanium background found in Bs is in line with that from
135 other studies and model predictions (Josko and Oleszczuk, 2013; Kim et al. 2012; Sun et al.
136 2014). Heavy metals (As, Cd, Cr, Hg, Ni and Pb), PAH (polycyclic aromatic hydrocarbons)
137 and *Salmonella spp.* content were all below the limit of law reference for its use in farm soils
138 (Italian Legislative Decree 99/92 and Commission Regulation (EU) n° 1357/2014).
139 Commercial powder of TiO_2 was bought from US Research Nanomaterials Inc. (Houston,
140 USA) as anatase or rutile NPs (nominal size of 30 nm) and from Sigma-Aldrich (Saint Louis,
141 USA) as bulk particles (>100 nm), all having at least 99.9% of purity (producers'
142 information).
143 Different growth substrates were prepared and designed as follows: 1) C1 = farming soil; 2)
144 C2 = farming soil enriched with 3% of Bs (dry weigh basis); 3) A = C2 + nano anatase; 4) R
145 = C2 + nano rutile; 5) Mix = C2 + anatase + rutile (1:1 ratio); 6) B = C2 + bulk TiO_2. For the
146 preparation of growth substrates 3) – 6) TiO_2 in nano and bulk sizes were suspended, at
147 appropriate concentrations, in milli-Q water using a sonicator (Sonifier 250, Branson) for 30
148 min at 80 W to simulate, through the Bs amendment, low and high dose TiO_2 loading in the
149 soil (80 and 800 mg TiO_2 kg^{-1} of soil, respectively). TiO_2 concentrations were chosen as
150 representative amounts of best- and worst-case scenarios of nanoparticles load through

151 biosolids in farm soils (Sun et al. 2014). TiO_2 suspensions and Bs were mixed mechanically
152 for 24 hs and left in open-air for 30 d with occasional mixing to permit the possible nano or
153 bulk particles transformations in the biosolid and the evaporation of excess water. The
154 resulting substrate material (Bs+TiO_2) was blended with the agricultural soil to obtain the
155 growth substrates A, R, Mix and B with nominal TiO_2 concentrations of 80 and 800 mg kg^{-1}
156 soil (dry-weight basis). C2 control soil was subjected to the same procedure without the TiO_2
157 addition. In comparison with C1, the C2 displayed increase of some agronomical parameters:
158 OM (3.1 times), CEC (1.5 times), EC (2.6 times), N_{tot} (5.7 times), P_{tot} (14.7 times), Ca (1.4
159 times), Mg (2.3 times), Cu (7.4 times) and Zn (4.1 times). Moreover, the pH was slightly
160 reduced to neutrality (7.01) and the texture remained unaltered.
161
162 *2.2 Plant material and growth conditions*
163 *Pisum sativum* L. seeds, homogeneously selected, were soaked in water over night and then
164 transferred to pots containing 500g of the growing substrates described above. Four pots per
165 treatment sowed with ten seeds per treatment were randomly disposed in a growth-room
166 under controlled conditions (16/8 h light/dark photoperiod, 22/16 °C) re-adjusting daily the
167 moisture of growth substrate with tap water. After 28d, plants were collected and root length
168 was measured. The roots were isolated, carefully washed with tap water and rinsed with
169 deionized water. Possible adhered soil particles in the roots were further eliminated by
170 sonication in deionized water using a pulse mode and an output power of 15W for about
171 5min. Fresh root samples were used for histochemical analysis, fixed for structural and
172 ultrastructural observations or stored at -80°C until use for biochemical determinations.
173
174 *2.3 Ti analysis in soils and plants*
175 The fraction of Ti available in soils, determined through a single extraction with

176 diethylenetriaminepentaacetic acid (DTPA), represents an operational method for the
177 determination of the fraction potentially accessible for plants uptake (Rauret 1998).
178 This bioavailable portion of Ti in the different growth substrates was determined using 0.01M
179 DTPA, following the procedure in Methods of Soil Analysis (SSSA 1996). Soil extracts were
180 volume reduced until almost dryness before Ti analysis. A portion of well-washed roots was
181 oven-dried and grounded to fine powder. Both, soil extracts and roots samples, were
182 mineralized in an open-block-digestor in two steps: after digestion with HNO_3 + H_2O_2, the
183 volume of liquid was reduced to almost dryness and the residue was re-digested with H_2SO_4
184 (Fang et al. 2009). Ti in the digested samples was determined by Inductively Coupled Plasma
185 Optical Emission Spectrometry (ICP-OES, Varian Liberty Axial). Control and assurance of Ti
186 analysis by ICP-OES were performed testing the two standard solutions (0.5 and 2 mg L-1)
187 every 5 samples. The same TiO_2 NPs employed in the experiments (Houston, USA) have
188 been used as a reference material for digestion method and Ti analysis, where the recovery
189 level (as TiO_2) ranged from 91% to 103% with a relative standard deviation of the mean of
190 2.95.
191
192 *2.4 Histochemical detection of oxidative stress on root system*
193 Five roots of comparable size and length, randomly selected from control and treated plants,
194 were excised and sectioned with hand microtome in correspondence to the initial root hair
195 area. Cross sections were immediately processed with fluorescent probes specific for
196 hydrogen peroxide and lipid peroxidation. Fluorescent Amplex UltraRed Reagent (Life
197 Technologies, USA) was applied for *in situ* detection of H_2O_2 following manufacturing
198 instructions and protocol reported in Ruffini Castiglione et al. (2016). After staining, slices
199 were mounted in glycerol and observed with fluorescence microscope (568ex/681em nm).
200 BODIPY 581/591 C11 was used as free radical sensor to visualize lipid peroxidation levels as

201 a change of the fluorescence emission peak from red to green. The slices were incubated and
202 stained following a previous protocol (Ruffini Castiglione et al. 2016). Microscope evaluation
203 was performed acquiring simultaneously the green (485ex/510em nm) and the red
204 fluorescence (581ex/ 591em nm) signals and merging the two images (Kovácik et al. 2014).
205 Fluorescence microscope analysis was carried out with a Leica DMLB, equipped with
206 appropriate set of excitation/emission filters and with a Leica DC300 ccd camera.
207
208 *2.5 Extraction and determination of hydrogen peroxide and thiobarbituric acid reactive*
209 *substances (TBARS)*
210 Hydrogen peroxide content of roots was determined according to Jana and Choudhuri
211 (1982). Briefly, roots were ground in a mortar and homogenised with phosphate buffer 50
212 mM pH 6.5. The homogenate was centrifuged at 6,000 g for 25 min. To determine the
213 H_2O_2 content, 3 ml of extracted solution were mixed with 1 ml of 0.1% titanium chloride in
214 20% (v/v) H_2SO_4, then the mixture was centrifuged at 6,000 g for 15 min and the
215 supernatant absorbance was read (410 nm). The amount of H_2O_2 in the extracts was
216 calculated from a standard curve and expressed as µmol g^{-1}FW.
217 Lipid peroxidation in roots was measured by detecting the amount of TBARS determined
218 by the thiobarbituric acid (TBA) reaction, according to Hartley-Whitaker et al. (2001) with
219 minor modifications as in Ruffini Castiglione et al. (2016). Briefly, roots were mixed with
220 TBA reagent (10% w/v trichloroacetic acid + 0.25% w/v thiobarbituric acid), heated (95°C
221 for 30 min), cooled for 15 min and centrifuged at 2,000 g for 15 min. The level of TBARS
222 was measured as specific absorbance at 532 nm by subtracting the non-specific absorbance
223 at 600 nm and calculated using an extinction coefficient of 155 mM^{-1} cm^{-1}. TBA-reactive
224 materials were expressed in nmol g^{-1} FW.
225

226 *2.6 Transmission electron microscopy (TEM)*

227 In order to evaluate morphology and size of nanoparticles, suspensions in milli-Q water were
228 prepared at 80 mg kg^{-1} and a drop (10 μL) was placed on TEM grids covered with formvar
229 and allowed to settle. The grids were stained with uranyl acetate, washed and left to dry. For
230 root observations, small root cubes (2x2 mm) of control and of each treatment were pre-fixed
231 in Karnovsky solution (Karnovsky 1965), post-fixed in osmium tetroxide, dehydrated and
232 embedded in Epon 812-Araldite A/M mixture. Thin sections were stained with uranyl acetate
233 and lead citrate.

234 Isolated NPs and root sections were observed under a FEI Technai electron microscope at
235 100kv.

236

237 *2.7 Statistical analysis*

238 Statistical analysis was performed using the Statistica package (StatSoft) version 6.0. All the
239 data were the mean of at least three replicates from three independent experiments. The
240 differences among means of the two control samples (C1 and C2) were compared using T
241 student test. Effects of treatments (form: anatase and rutile; size: nano and bulk), of the two
242 concentrations and their interaction were analyzed using two-way ANOVA. The differences
243 among means were compared with a *post-hoc* analysis of variance using Tukey test (Tukey
244 Honestly Significant Difference) at $p < 0.05$.

245

246 **3. Results**

247 *3.1 Titanium in soils and roots*

248 Titanium analysis in the soil extracts and in the biomass of roots were represented in Fig 1.
249 The concentration of Ti bioavailable in the soils ranged from 290 to 625 μg kg^{-1}. The
250 presence of biosolid did not affect the available fraction of Ti in the soil since no significant

251 differences were observed between C1 and C2. Ti spiking (through the Bs soil amendment)
252 induced significant differences in Ti content in the soil in function of different treatments
253 (F=13.91, P<0.001) and concentrations (F=27.97, P<0.001), particularly evident for A800
254 showing a significant increase (about 70%) in respect to C2 (Fig. 1). Statistical significant
255 interaction between treatments and concentration (F=11.25, P<0.001) was observed.
256 Titanium accumulation in the roots (Fig. 1) was similar in the C1, C2 and in the roots from
257 low dose in all the treatments, with significantly higher accumulation than C2 found in all the
258 high dose treatments (F=74.935, P<0.0001), R800 and B800 displaying differences with
259 statistical significance.
260
261 *3.2 Root growth and oxidative stress*
262 After 28 days, C2 plants displayed reduced root length in comparison to C1 plants (Table 1a).
263 Moreover, our data indicated a further significant root growth inhibition under TiO_2
264 treatments (F=13.154, P<0.0001), the lowest value characterising A80, followed by B800 and
265 B80 (Table 1b), with no significant effect for concentration (F=2.475, P=0.119) and
266 interaction between the two factors (F=2.348 P=0.0589).
267 In Table 1a not significant differences in H_2O_2 content between the roots of the two controls
268 were observed. In comparison with C2, all the treated materials had higher concentration of
269 this signalling molecule (Table 1b), in function of treatments (F=9.967, P<0.0001) and
270 concentration (F=16.468, P<0.0001), the highest content being reached in A80, followed by
271 Mix80, B800 and R800 (in decreasing order). The lowest content of H_2O_2 was observed in
272 Mix800. A significant interaction was observed between the two factors (F=24.078,
273 P<0.0001).
274 C2 and C1 had comparable concentrations of TBARS, indicative of lipid peroxidation and of
275 membrane damage (Table 1a). NPs treatments significantly influenced TBARS content

276 (F=12.257, P<0.0001), Mix800 showing the highest concentration of TBARS and the other
277 treatments having lower values than C2 except for A80 and Mix 80. No significant effect was
278 distinguished for concentrations (F=0.3103, P=0.582), while a significant interaction was
279 observed between the two factors (F=4.752, P<0.0001) (Table 1b).
280
281 *3.3 Histochemical analyses*
282 Specific fluorescent probes were exploited for *in situ* detection of H_2O_2 and lipid peroxidation
283 to achieve qualitative signals related to the oxidative stress.
284 After Amplex UltraRed probe staining (Fig. 2), root cross sections of C1 and C2 samples
285 showed both a faint signal in the cortical cylinder, except for the endodermis, that resulted
286 distinctly stained in the portions facing towards phloem arcs in C2 sample. Central cylinder
287 was more reactive in C2 samples both in the phloematic and mostly in the xylematic arcs.
288 R80 displayed similarity with the C1 staining pattern with reference to the central cylinder,
289 even if in the cortical cylinder the red signal was restricted at the area surrounding the stele.
290 At the high TiO_2 dose treatments, rutile (R800) induced high levels of H_2O_2 in the central
291 cylinder, especially in phloem tissues, and in the inner part of cortical cylinder.
292 A80 and A800 root cross sections displayed a staining pattern strongly involving phloem
293 tissues, and, to a lesser extent, xylem vessels and cortical area, with a high overall staining
294 intensity in A80 samples.
295 Mix800 was the less reactive sample to Amplex UltraRed staining, with a faint signal
296 engaging basically the vascular tissue system, accompanied by uneven weaker signal on the
297 cortical cylinder. Mix80, on the contrary, showed a greater signal intensity in all root
298 compartments extended to the cortical cylinder, including the endodermic layer, facing
299 towards the phloematic arches, and vascular tissues.

300 The roots belonging to plants treated with B80 and B800 mainly showed positivity to the
301 H_2O_2 fluorescent probe in the inner part of cortical cylinder and a peculiar strong staining
302 signal in the rizodermis. Vascular tissue system was as well responsive, especially the phloem
303 tissues of B800.
304 BODIPY 581/591 C11 fluorescent probe is able to identify lipid peroxidation as a change of
305 the fluorescence emission peak from red to green. C1 and C2 samples showed a faint green
306 signal restricted to the cortical region closest to the root central cylinder (Fig. 3). The green
307 fluorescence was observed in the same root compartment in the samples A80, Mix800 and
308 Mix80. In this latter, the green signal also spread the central cylinder. A800 and R800
309 displayed a preferential green staining to the central cylinder, involving also vascular system
310 as well as the inner part of the cortex. R80 sample was the most similar to C2. B80 and B800
311 reacted to the fluorescent probe with a different pattern of staining, that was mainly
312 recordable in the outer and inner portion of the cortical cylinder (Fig. 3).
313
314 *3.4 TEM observations*
315 The TiO_2 anatase NPs (Fig. 4a) were extremely heterogeneous in shape, generally they
316 appeared prismatic or cylindrical in shape; their size was variable from 20 to 80 nm. The
317 rutile NPs were prismatic with cusp and size from 30 to 100 nm (Fig. 4b). Both anatase and
318 rutile NPs appeared highly aggregate.
319 Sections of C1 roots showed cells with large vacuoles with scanty materials evident (Fig. 4c).
320 The thin layer of cytoplasm was rich in endoplasmic reticulum cisternae, dictyosomes,
321 mitochondria and plastids (Fig. 4c).
322 The cells of samples grown in C2 showed ultrastructure similar to that of cells of C1. Often
323 the chromatin was condensed and mitochondria had swollen cristae (Fig. 4d). Some NPs of
324 size 30-50 nm were observed adherent to cellular walls mainly in parenchyma (cortex) cells

325 near to central cylinder (Fig. 4e). In the parenchyma (cortex) cells near to rizoderma
326 aggregates of dense particles (up to 100 nm) were evident (Fig. 4f).
327 In R treated roots cells were often empty or showed more or less evident plasmalemma-wall
328 detachment as in plasmolysis. In the vacuoles of these cells disperse materials and dense NPs
329 of about 20-30 nm were present (Fig. 5a). Furthermore, in these vacuoles wide zones of
330 degenerated cytoplasm were present, often surrounded by a double membrane, with not
331 recognizable organelles and more or less large vesicles containing dense round profiled NPs
332 of about 30 nm in size (Fig. 5b).
333 In A treated roots cells appeared empty or in evident plasmolysis state, as R treated roots cells.
334 Not recognizable organelles or mitochondria with swollen *cristae* and with large crystals (Fig.
335 5c) and nuclei with highly condensed chromatin were evident (Fig. 5d). NPs single or
336 aggregated of about 20-40 nm in size were present in the cytoplasm (Fig. 5e). In vacuoles
337 scattered material with NPs of about 30 nm in size, and vesicles surrounded by a double
338 membrane containing NPs of the same dimension were present (Fig. 5f). In the parenchyma
339 (cortex) cells near to rizoderma, NPs of 20-50 nm in size were observed in organelles,
340 probably mitochondria (Fig. 6a) in portions of cytoplasm (Fig. 6b), adherent or crossing cell
341 wall (Fig. 6c) and in intercellular spaces (Fig. 6d).
342 The cell ultrastructure of Mix treated roots were similar to that described for both A and R
343 treated root cells, namely: evident plasmolysis and disrupted cytoplasm and organelles. The
344 NPs were dispersed in vacuoles, in vesicles surrounded by a double membrane and in
345 cytoplasm (data not shown).
346 The cells of B treated roots were mostly empty, the only organelles detected were the nuclei,
347 often in number of two *per* cell (Fig. 6e). Large nanoparticles and particles of different
348 polyhedral form, isolated or aggregated, were present in parenchyma (cortex) cells near to
349 rizoderma (Fig. 6f).

350 No differences in ultrastructure and NPs content were noted in all the samples treated with the
351 two different concentrations.
352
353
354 **4. Discussion**
355 Our study focused on crop plant response to a simultaneous exposure to biosolid and TiO_2 at
356 micro- and nano-scale, whose co-presence may really occur in farm soils (Chen et al. 2017).
357 Generally, the soil treatments with Bs and Bs+TiO_2 did not significantly modify the Ti
358 available fraction in soils, indicating, in this respect, a non-substantial influence of the
359 amendment/spiking on the growth matrix. Exception was found for A800, suggesting a lower
360 entrapment or precipitation of anatase NPs as homo/hetero-aggregates with soil components
361 and producing a significant increase in the Ti bioavailable. Indeed, in soils, the association of
362 multiple factors, including their inorganic and organic constituents and the crystallographic
363 features of NPs, has been reported as the drivers for the TiO_2 behaviour and availability
364 (Laxma Reddy et al. 2016; Tassi et al. 2012).
365 Even if Ti is not an essential nutrient element, in our experimental conditions *P. sativum* roots
366 were able to accrue Ti at concentration levels in some respects even higher than specific
367 essential mineral elements (Lyu et al. 2017) and this was generally recorded regardless of the
368 presence of Bs or nano (and bulk) TiO_2 particles in soil. Only at the high dose treatments *P.*
369 *sativum* roots increased at a certain extent their Ti content, the statistical significance being
370 limited to R800 and B800.
371 The effect of TiO_2 treatments on the root growth of *P. sativum* differed mainly depending on
372 the crystalline form. In accordance with Pittol et al. (2017), TiO_2 NPs treatments induced a
373 reduction in the root growth and the inhibiting action of the micro-scale form (bulk) was
374 confirmed (Ruffini Castiglione et al. 2016). At the low dose treatments, anatase was more

375 toxic than rutile for growth, confirming the higher toxicity of this crystal form in these
376 conditions (Siddiqi and Husen 2017). On the other hand, it must be emphasized that the high
377 dose treatments induced a less negative effect on root elongation, however, significant only
378 for anatase. The mitigation of anatase phytotoxic effect at high concentration has been
379 reported in literature and could be due to the suggested antimicrobial properties of this
380 crystalline form, which increases plant stress resistance (Zheng et al. 2005; Siddiqi and Husen
381 2017). The total Ti content in the root did not differ respect to the controls, despite the
382 increase in the availability of Ti recorded in A800. These results suggest that a multifaceted
383 mechanism of TiO_2 action is present in a such complex matrix, as is the Bs-amended soil, and
384 that it is difficult to foresee/hypothesize the effects which can result in opposite and
385 compensatory responses of the plant.
386 A correlation between the inhibition of growth and the generation of reactive oxygen species
387 (ROS), resulting in oxidative stress, has often been suggested (Prakash and Chung 2016). This
388 was only partially confirmed in our results, where the highest H_2O_2 concentration was
389 associated with the highest inhibition of root growth just in some samples. In fact a non-
390 typical dose-effect relationship for oxidative stress markers seemed to characterize the plant
391 response in our experimentation, probably not weird for NPs spiked into a complex growth
392 matrix (Bell and Ives 2014; Simonin et al. 2016). In addition, and in contrast with Ruffini
393 Castiglione et al. (2016), the highest contents of this ROS were not associated with the
394 highest membrane damages (assessed as TBARS).
395 To complement structure-function analysis, within a project based on an integrated approach,
396 interesting information may derive from the histochemical detection of oxidative stress and
397 the electron microscopy approach, that, though providing semiquantitative/qualitative data,
398 can highlight any differences in the pattern and distribution of oxidative markers, as well as in
399 the cell ultrastructure.

400 Histochemical data, in some respects remind biochemical quantitative results, basically with
401 no specific differences between C1 and C2 samples for both the probes; notwithstanding this,
402 H_2O_2 staining pattern seems more defined for C2 sample, indicating an H_2O_2 production not
403 limited to a normal aerobic metabolism or physiological signalling processes.
404 This behaviour in C2, together with the significant inhibition of root growth, could be
405 ascribed to elements as Cu and Zn that, in accordance with literature (Wen et al. 2002),
406 increased compared to the original soil, of 7.4 times and 4.1 times respectively. These
407 elements notoriously affect the root elongation (Muccifora 2008; Li et al. 2012) and H_2O_2
408 content (Thounaujam et al. 2012; Li et al. 2013). Equally, non-humified compounds resulting
409 from an incomplete biodegradation of organic matter from Bs, such as phenols and ammonia,
410 could cause toxicity in plants (Britto and Kronzucker 2002; Zubillaga and Lavado 2006).
411 Moreover, in C2, NPs of 30-50 nm and large dense particles recorded by TEM analysis and
412 never relieved in C1, could come from the biosolid and be responsible of feeble ultrastructural
413 and histochemical differences between the two controls.
414 The addition of TiO_2 NPs to C2 growth substrates induced distinct histochemical staining
415 patterns allied to H_2O_2 and lipid peroxidation, relating to specific root compartments and
416 depending on the different treatments. These results, in addition with biochemical quantitative
417 data, provide further useful clues, that allow to reveal differences not appreciable with a mere
418 quantitative approach and demonstrating that plant root tissues are differently affected
419 depending on the different TiO_2 crystalline form. For the plants treated with nanoTiO_2 the
420 location of H_2O_2 signal in the cortical cylinder in general corresponds to the lipid peroxidation
421 pattern by the BODIPY probe. The apparent contradiction with biochemical results, that
422 seemed to exclude a clear correlation between hydrogen peroxide concentration and TBARS
423 content, further highlights the importance of a multiple approach to better characterize the
424 actual condition of plant material. Interestingly, H_2O_2 positive signal was recurrently

425 observed in correspondence of the vascular tissues. Xylem parenchyma cells supply the H_2O_2
426 required for lignification in differentiating xylem vessels (Barceló 2005). H_2O_2 production
427 and cell-wall lignification increase as oxidative stress response (Kim and Barbara 2008), in
428 our case particularly evident for C2, A80, Mix80 treatments. The presence of H_2O_2 in phloem
429 tissues may be a possible occurrence, being previously described following biotic stress
430 (Walz et al 2002; Musetti et al. 2005) as well as elicited by TiO_2 nanoparticles (Ruffini
431 Castiglione et al. 2016). This occurring may be the result of a systemic stress responses
432 (Wendehenne et al. 2014) in which phloem is involved, changing its transport capacity and
433 the type of molecules/gene products moved (Petrov and Van Breusegem 2012; Liang et al.
434 2014).
435 Although the ultrastructural pattern did not highlight differences depending on the
436 concentration of TiO_2 particles, TEM analysis turned out to be a precocious marker of further
437 evident damages, allowing a fine-tune monitoring of the cell/tissue response to TiO_2 NPs.
438 The electron microscope observation corroborated the presence of both anatase and rutile
439 NPs, confirming their ability to overcross plant root barriers and penetrate the different
440 root/cell compartments (Wang et al. 2016). The most damaged root areas generally
441 corresponded to those identified by histochemical analysis and cell and chromatin
442 ultrastructure appeared more harmed in A than in R treated samples, confirming, also with
443 this approach, the highest toxicity of anatase crystals in plants (Siddiqi and Husen 2017) or
444 minor ability of their detoxification.
445 Indeed, based on our results, we could hypothesise that the toxicity of TiO_2 NPs may depend
446 on the cell ability to isolate them in subcellular compartments, avoiding their interaction with
447 organelles and/or metabolic processes. Though a fraction of anatase NPs was confined in
448 vesicles and in autophagosome-like structures, as previously shown in response to NPs stress
449 (Ruffini Castiglione et al. 2016), most of them was observed free in the cytoplasm and in

450 degenerating organelles as if the ability of the detoxification system was exceeded. On the
451 contrary, vacuole sequestration mechanisms of rutile NPs in *P. sativum* root seemed to work
452 in a more efficient way, even when Ti concentration almost doubled (R800), avoiding
453 interaction of these particles with subcellular components and cell metabolism and moreover
454 limiting the damages already received.
455 The response of the Mix treated samples recalled that of A treated samples not only for root
456 growth inhibition, and oxidative stress but also concerning ultrastructural data. These findings
457 can be explained on the basis of the possible influence of the more toxic anatase inside the
458 Mix treatment.
459 Though biochemical quantitative data of bulk treated roots did not show a correspondence
460 between hydrogen peroxide and TBARS contents, histochemical analysis highlighted a
461 superimposable signal pattern by the two specific probes, suggesting a H_2O_2-dependent
462 membrane damage. The fluorescence signals were distinctive in respect to the other
463 treatments, mainly confined in the root epidermis as well as the outermost and innermost
464 layers of the cortex.
465 A strong H_2O_2 signal in the outer part of root cortex was previously noticed (Ruffini
466 Castiglione et al. 2016) in short-term studies in *V. faba* treated with bulk TiO_2 suspension,
467 indicating this part of the root as a preferential target of the micro-scale TiO_2 particles. Just in
468 that root portion, in our system, nanoparticles and particles of different form and aggregation
469 status were detected by TEM analysis. These nanoparticles could be derived from the biosolid,
470 as already relieved for C2. The cell ultrastructure, characterized mainly by empty cells and
471 often presence of two nuclei, suggested alterations of the division cellular process probably on
472 the phragmoplast formation and microtubules. TiO_2 B material, considered for decades an
473 inert and safe material, conversely confirmed its harmfulness (Ruffini Castiglione et al. 2016),

474 inducing genotoxic effects and extensive cell death, according to its classification as possibly
475 carcinogenic to humans (Group 2B carcinogen, IARC 2010).
476
477 **5. Conclusions**
478
479 These findings allow us to conclude that, in our experimental conditions, the presence of
480 biosolid disturbs plant growth of *P. sativum*, causing cellular damages at root level probably
481 through mechanisms not only oxidative stress-dependent, and involving altered signalling
482 processes. These disturbances may depend on non-humified compounds and/or on the
483 presence of toxic elements and of NPs in the Bs-amended soil, being biosolid one of the
484 major sink of TiO_2 NPs released into the soil environment.
485 The addition of TiO_2 particles in the sludge-amended soil further alters plant growth and
486 elicits oxidative and ultrastructural damages. However, non-typical dose-effect relationship
487 seemed to characterize the plant response in our experimentation, suggesting that the
488 complexity of the Bs-amended soil matrix makes it difficult to foresee particle behaviour and
489 effects on plant. In this context, an integrated approach is particularly useful allowing a
490 complementary structure-function analysis.
491 The most responsiveness treatments were those conducted by the anatase crystal form, alone
492 or mixed with rutile, as well as by the corresponding bulk material, whose inhibiting action
493 was confirmed.
494 Both TiO_2 crystal forms were taken up and compartmentalized by plant cell as a possible
495 defence mechanism, particularly effective for rutile NPs.
496 The results of our work suggest a reflection on the promising use of soil amendments and on
497 the application of nanomaterials and their safety. These practices should be carefully analysed,

to establish right regulations over their use, confinement, and disposal for the environmental protection and living organism health.

Acknowledgments

This work was financed by local funding of the University of Pisa (ex 60%) and supported by University of Siena and National Research Council of Italy.

504 **References**

505 Amini S, Maali-Amiri R, Mohammadi R, Kazemi-Shahandasht SS (2017) cDNA-AFLP
506 analysis of transcripts induced in chickpea plants by TiO_2 nanoparticles during cold stress.
507 Plant Physiol Biochem 111: 39-49

508 Bakhshizadeh M, Sazgarnia A, Seifi M, Hadizadeh F, Rajabzadeh G, Mohajeri SA (2017)
509 TiO_2-based mitoxantrone imprinted poly (Methacrylic acid-co-polycaprolctone
510 diacrylate) nanoparticles as a drug delivery system. Curr Pharm Des 23: 2685-2694

511 Barceló AR (2005) Xylem parenchyma cells deliver the H_2O_2 necessary for lignification in
512 differentiating xylem vessels. Planta 220: 747–756

513 Bell IR, Ives JA (2014) Nonlinear effects of nanoparticles biological variability: biological
514 variability from hermetic doses, small particles sizes, and dynamic adaptive interactions.
515 Dose-Response 12: 202–232

516 Bhawana P, Fulekar MH (2012) Nanotechnology: remediation technologies to clean up the
517 environmental pollutants. Res J Chem Sci 2: 90-96

518 Brar SK, Verma M, Tyagi RD, Surampalli RY (2010) Engineered nanoparticles in wastewater
519 and wastewater sludge – Evidence and impacts. Waste Manage 30: 504–520

520 Britto DT, Kronzucker HJ (2002) NH_4^+ toxicity in higher plants: a critical review. J Plant
521 Physiol 159: 567-584

522 Burke DJ, Zhu S, Pablico-Lansigan MP, Hewins CR, Samia ACS (2014) Titanium oxide
523 nanoparticle effects on composition of soil microbial communities and plant
524 performance. Biol Fert Soils 50: 1169–1173

525 Chen C, Tsyusko OV, McNear Jr. DH, Judy J, Lewis RW, Unrine JM (2017) Effects of
526 biosolids from a wastewater treatment plant receiving manufactured nanomaterials on
527 *Medicago truncatula* and associated soil microbial communities at low nanomaterial
528 concentrations. Sci Total Environ 609: 799–806

529 Chuankrerkkul N, Sangsuk S (2008) Current status of nanotechnology consumer products and
530 nano-safety issues. JMMM 18: 75–79
531 Commission Regulation (EU) No 1357/2014 of 18 December 2014 replacing Annex III to
532 Directive 2008/98/EC of the European Parliament and of the Council on waste and
533 repealing certain Directives; https://eur-lex.europa.eu/legal-
534 content/EN/TXT/?uri=CELEX%3A32014R1357, accessed in June 2018
535 Cox A, Venkatachalam P, Sahi S, Sharma N (2016) Silver and titanium dioxide nanoparticle
536 toxicity in plants: A review of current research. Plant Physiol Biochem 107: 147-163
537 Du W, Sun Y, Ji R, Zhu J, Wu J, Guo HJ (2011) TiO_2 and ZnO nanoparticles negatively
538 affect wheat growth and soil enzyme activities in agricultural soil. J Environ Monit 13:
539 822-828
540 El-Sherbiny S, Morsy F, Samir M, Fouad OA (2014) Synthesis, characterization and
541 application of TiO_2 nanopowders as special paper coating pigment. Appl Nanosci 4:
542 305–313
543 Fang J, Shan X, Wen B, Lin J, Owens G (2009) Stability of titania nanoparticles in soil
544 suspentions and transport in saturated homogeneous soil columns. Environ Poll 157:
545 1101-1109
546 Gogos A, Moll J, Klingenfuss F, van der Heijden M, Irin F, Green MJ, Zenobi R, Bucheli TD
547 (2016) Vertical transport and plant uptake of nanoparticles in a soil mesocosm
548 experiment. J Nanobiotech 14: 40
549 Halden RU (2015) Epistemology of contaminants of emerging concern and literature meta-
550 analysis. J Hazard Mat 282: 2-9
551 Hartley-Whitaker J, Ainsworth G, Meharg AA (2001) Copper- and arsenate-induced
552 oxidative stress in *Holcus lanatus* L. clones with differential sensitivity. Plant Cell
553 Environ 24: 713-722

554 EEC (1986) http://ec.europa.eu/environment/waste/sludge/index.htm. Council Directive
555 86/278/EEC on "The protection of the environment, and in particular of the soil, when
556 sewage sludge is used in agriculture"
557 EPA (1994) https://www.epa.gov/biosolids/biosolids-recycling-beneficial-technology-better-
558 environment. 832-R-94-009 on "Biosolids Recycling: Beneficial Technology for a
559 Better Environment"
560 EPA (1993) https://www.epa.gov/biosolids/biosolids-laws-and-regulations#compliance. On
561 "Wastewater Management".
562 IARC—International Agency for Research on Cancer, 2010. Monographs 93. Titanium
563 Dioxide. http://monographs.iarc.fr/ENG/Monographs/vol93/mono93-7.pdf.
564 Italian Legislative Decree n°99/1992, Implementation of Directive 86/278 / EEC, concerning
565 the protection of the environment, in particular of the soil, in the use of sludge in
566 agriculture, Official Gazette, No. 38, 15 February 1992, Ordinary Supplement No. 28.
567 Jana S, Choudhuri MA (1982) Glycolate metabolism of three submerged aquatic angiosperm
568 during aging. Aquatic Bot 12: 345-354
569 Josko I, Oleszczuk P (2013) The influence of ZnO and TiO_2 nanoparticles on the toxicity of
570 sewage sludges. Environ Sci Processes and Impacts 15: 296-306
571 Karnovsky MJ (1965) A formaldehyde-glutaraldehyde fixative of high osmolality for use in
572 electron microscopy. J Cell Biol 27: 137-138
573 Kim B, Murayama M, Colman BP, Hochella F Jr (2012) Characterization and environmental
574 implications of nano- and larger TiO_2 particles in sewage sludge, and soils amended
575 with sewage sludge. J Environ Monitor 14: 1129-1137
576 Kim HJ, Triplett B (2008) Involvement of extracellular Cu/Zn superoxide dismutase in cotton
577 fiber primary and secondary cell wall biosynthesis. Plant Signal Behav 3: 1119–1121
578

579 Kovácik J, Babula P, Hedbavny J, Švec P (2014) Manganese-induced oxidative stress in two
580 ontogenetic stages of chamomile and amelioration by nitric oxide. Plant Sci 215-216: 1-
581 10
582 Larue C, Laurette J, Herlin-Boime N, Khodja H, Fayard B, Flank AM, Brisset F, Carriere M
583 (2012) Accumulation, translocation and impact of TiO_2 nanoparticles in wheat (*Triticum*
584 *aestivum* spp.): influence of diameter and crystal phase. Sci Total Environ 431: 197–208
585 Laxma Reddy PV, Hernandez-Viezcas J-A, Peralta-Videa JR, Gardea-Torresdey JL (2016)
586 Lessons learned: are engineered nanomaterials toxic to terrestrial plants? Sci Total
587 Environ 568: 470–479
588 Li X, Yang Y, Jia L, Chen H, Wei X (2013) Zinc-induced oxidative damage, antioxidant
589 enzyme response and proline metabolism in roots and leaves of wheat plants.
590 Ecotoxicol Environ Saf 89: 150–157
591 Li X, Yang Y, Zhang J, Jia L, Li O, Zhang T, Qiao K, Ma S (2012) Zinc induced
592 phytotoxicity mechanism involved in root growth of *Triticum aestivum* L. Ecotoxicol
593 Environ Saf 86: 198-203
594 Liang D, White RG, Waterhouse PM (2014) Mobile gene silencing in *Arabidopsis* is
595 regulated by hydrogen peroxide. PeerJ 2:e701; DOI 10.7717/peerj.701
596 Liu WK (2011) TiO_2-NPs application in agriculture: a review. In *Agricultural Research*
597 *Updates* (ed B.P. Hendriks), pp. 137–145. Nova Publisher, Hauppage, New York
598 Lu Q, He ZL, Stoffella PJ (2012) Land application of biosolids in the USA: a review. Applied
599 and Environmental Soil Science 2012 : Article ID 201462
600 http://dx.doi.org/10.1155/2012/201462
601 Lyu S, Wei X, Chen J, Wang C, Wang X, Pan D (2017) Titanium as a beneficial element for
602 crop production. Front Plant Sci 8: 597

603 Maurer-Jones MA, Ian L, Gunsolus IL, Murphy KJ, Haynes CL (2013) Toxicity of
604 engineered nanoparticles in the environment. An Chem 85: 3036–3049
605 Muccifora S (2008) Effects of copper on spore germination, growth and ultrastructure of
606 *Polypodium cambricum* L. gametophytes. Environ Poll 153: 369-375
607 Musetti R, Sanità di Toppi L, Martini M, Ferrini F, Loschi A, Favali MA, Osler R (2005)
608 Hydrogen peroxide localization and antioxidant status in the recovery of apricot plants
609 from European Stone Fruit Yellows. Eur J Plant Pathol 112: 53–61
610 Pachapur VL, Larios AD, Cledón M, Brar SK, Verma M, Surampalli RY (2016) Behaviour
611 and characterization of titanium dioxide and silver nanoparticles in soils. Sci Total
612 Environ 563–564: 933–943
613 Petrov VD, Van Breusegem F (2012) Hydrogen peroxide-a central hub for information flow
614 in plant cells. AoB PLANTS pls014; DOI:10.1093/aobpla/pls014
615 Pittol M, Tomacheski D, Simões DN, Ribeiro VF, Santana CRM (2017) Macroscopic effects
616 of silver nanoparticles and titanium dioxide on edible plant growth. Environ Nanotech
617 Monit Manag 8: 127-133
618 Prakash MG, Chung IM (2016) Determination of zinc oxide nanoparticles toxicity in root
619 growth in wheat (*Triticum aestivum* L.) seedlings. Acta Biol Hung 67: 286–296.
620 Rauret G (1998) Extraction procedures for the determination of heavy metals in contaminated
621 soil and sediment. Talanta 46: 449-455.
622 Remédios C, Rosário F, Bastos V (2012) Environmental nanoparticles interactions with
623 plants: morphological, physiological, and genotoxic aspects. J Botany 2012: Article ID
624 751686, http://dx.doi.org/10.1155/2012/751686
625 Rico CM, Majumdar S, Duarte-Gardea M, Peralta-Videa JR, Gardea-Torresdey JL (2011)
626 Interaction of nanoparticles with edible plants and their possible implications in the food
627 chain. J Agric Food Chem 59: 3485–3498

628 Ruffini Castiglione M, Cremonini R (2009) Nanoparticles and higher plants. Caryologia 62:
629 161–165
630 Ruffini Castiglione M, Giorgetti L, Cremonini R, Bottega S, Spanò C (2014) Impact of TiO_2
631 nanoparticles on *Vicia narbonensis* L.: potential toxicity effects. Protoplasma 251:
632 1471–1479
633 Ruffini Castiglione M, Giorgetti L, Bellani L, Muccifora S, Bottega S, Spanò C (2016) Root
634 responses to different types of TiO_2 nanoparticles and bulk counterpart in plant model
635 system *Vicia faba* L. Environ Exp Bot 130: 11–21
636 Siddiqi KS, Husen A (2017) Plant response to engineered metal oxide nanoparticles.
637 Nanoscale Res Lett 12: 92 DOI 10.1186/s11671-017-1861-y
638 Simonin M, Richaume1 A, Guyonnet JP, Dubost A, Martins JMF, Pommier T (2016)
639 Titanium dioxide nanoparticles strongly impact soil microbial function by affecting
640 archaeal nitrifiers. Sci Reports 6: 33643 | DOI: 10.1038/srep33643
641 Song U, Shin M, Lee G, Roh J, Kim Y, Lee EJ (2013) Functional analysis of TiO_2
642 nanoparticle toxicity in three plant species. Biol Trace Element Res 155: 93–103
643 SSSA book series (1996) In Methods of soil analysis, Part 3 - Chemical Methods (ed D.L.
644 Sparks), Soil Science Society of America Inc., Madison, USA
645 Sun TY, Gottschalk F, Hungerbühler K, Nowack B (2014) Comprehensive probabilistic
646 modelling of environmental emissions of engineered nanomaterials. Envir Poll 185: 69–
647 76
648 Tassi E, Giorgetti L, Morelli E, Peralta-Videa JR, Gardea-Torresdey JL, Barbafieri M. (2017)
649 Physiological and biochemical responses of sunflower (*Helianthus annuus* L.) exposed
650 to nano-CeO_2 and excess boron: Modulation of boron phytotoxicity. Plant Physiol
651 Biochem 110: 50-58

652 Tassi EL, Pini R, Gorini F, Valadao I, De Castro JA (2012) Chemical and physical properties
653 of soil influencing TiO_2 nanoparticles availability in terrestrial ecosystems. J Environ
654 Res Develop 6: 1014-1018
655 Thounaojam TC, Panda P, Mazumdar P, Kumar D, Sharma GD, Sahoo L, Panda S (2012)
656 Excess copper induced oxidative stress and response of antioxidants in rice. Plant
657 Physiol Biochem 53: 33-39
658 Tourinho P, van Gestel CA, Lofts S, Svendsen C, Soares AM, Loureiro S (2012) Metal-based
659 nanoparticles in soil: fate, behavior, and effects on soil invertebrates. Environ Toxic
660 Chem 31: 1679–1692
661 Villatte G, Massard C, Descamps S, Sibaud Y, Forestier C, Awitor KO (2015) Photoactive
662 TiO_2 antibacterial coating on surgical external fixation pins for clinical application. Inter
663 J Nanomed 10: 3367–3375
664 Walz C, Juenger M, Schad M, Kehr J (2002) Evidence for the presence and activity of a
665 complete antioxidant defence system in mature sieve tubes. Plant J 31: 189-197
666 Wang WK, Chen JJ, Zhang X, Huang YX, Li WW, Yu HQ (2016) Self-induced synthesis of
667 phase-junction TiO_2 with a tailored rutile to anatase ratio below phase transition
668 temperature. Sci Rep 6:20491 | DOI: 10.1038/srep20491
669 Weir A, Westerhoff P, Fabricius L, Hristovski K, von Goetz N (2012) Titanium dioxide
670 nanoparticles in food and personal care products. Environ Sci Technol 46: 2242−2250
671 Wen G , Bates TE, Inanaga S, Voroney RP, Hamamura K, Curtin D (2002) A yield control
672 approach to assess phytoavailability of Zn and Cu in irradiated, composted sewage
673 sludges and composted manure in field experiments: II. Copper. Plant Soil 246: 241–248
674 Wendehenne D, Gao QM, Kachroo A, Kachroo P (2014) Free radical-mediated systemic
675 immunity in plants. Curr Opin Plant Biol 20: 127–134

676 Yang Y, Wang Y, Westerhoff P, Hristovski K, Jin VL, Johnson MVV, Arnold JG (2014)
677 Metal and nanoparticle occurrence in biosolid-amended soils. Sci Total Environ 485–
678 486:441–449
679 Zheng L, Hong F, Lu S, Liu C (2005) Effect of nano-TiO_2 on strength of naturally aged seeds
680 and growth of spinach. Biol Trace Elem Res 104:83–91
681 Zubillaga MS, Lavado RS (2006) Phytotoxicity of biosolids compost at different degrees of
682 maturity compared to biosolids and animal manures. Compost Sci Util 14: 267–270
683
684
685

686 **Figure Legends**

687

688 **Fig. 1** Concentration of Titanium in the soil available fraction (left side axis) and in the root
689 tissues (right side axis) of *Pisum sativum* grown for 28 days in farming soil (C1), in C1
690 amended with biosolid (C2) and in the presence of 80 and 800 mg/Kg of TiO_2 nanoparticles
691 (anatase (A), rutile (R), mix anatase+rutile 1:1 ratio (Mix)) and bulk material (B). Values are
692 mean of n=3 replicates with standard deviation; different letters in the same matrix represent
693 significant differences ($p<0.05$), according to ANOVA and *post hoc* Tukey test. C1 and C2
694 were compared by Student's t-test ($p<0.05$).

695

696 **Fig. 2** Cross hand sections of *Pisum sativum* roots grown for 28 days in farming soil (C1); in
697 C1 amended with biosolid (C2) and in the presence of 80 and 800 mg/Kg of TiO_2
698 nanoparticles (anatase, rutile, mix anatase+rutile 1:1 ratio) and bulk material. The plate
699 comprehends representative images of toluidine blue stained root section and of *in situ*
700 detection of H_2O_2 by Amplex UltraRed Reagent.

701

702 **Fig. 3** Cross hand sections of *Pisum sativum* roots grown for 28 days in farming soil (C1); in
703 C1 amended with biosolid (C2) and in the presence of 80 and 800 mg/Kg of TiO_2
704 nanoparticles (anatase, rutile, mix anatase+rutile 1:1 ratio) and bulk material. The plate
705 comprehends representative images of toluidine blue stained root section and of *in situ*
706 detection of lipid peroxidation by BODIPY 581/591 C11.

707

708 **Fig. 4** TEM images of: **a**) aggregates of TiO_2 anatase nanoparticles (NPs); **b**) aggregates of
709 TiO_2 rutile NPs; **c**) portion of control (C1) root cell: the arrow indicates endoplasmic
710 reticulum; **d-f)** portion of C1 amended with biosolid (C2) root cells: **e**) the arrows indicate the

711 NPs adherent to cell wall near to central cylinder; **f**) the arrow indicates dense particles
712 aggregates in parenchima cells near to rizoderma. V, vacuole; M, mitochondrion; C,
713 chromathin; CW cell wall.
714
715 **Fig. 5** TEM images of **a**) nanoparticles (NPs) (arrows) in cell vacuole of rutile treated root
716 (R800 sample); **b**) portion of cell vacuole of rutile treated root: not recognisable organelles
717 (O) and vesicles (Ve) in zones surrounded by double membrane; the arrows indicate NPs
718 (R800); **c**-**e**) portions of anatase treated root cells, the arrowhead indicate a crystal in a
719 mitochondrion (M), the arrows indicate NPs in the cytoplasm (**c**: A800, **d**: A80; **e**: A80); **f**)
720 NPs (arrows) in vacuoles and in vesicles (Ve) in anatase treated cell root (A80). N, nucleus;
721 V, vacuole.
722
723 **Fig. 6** TEM images of **a, b**) portion of cells near to rizoderma of anatase treated roots, the
724 arrows indicate Nanoparticles (NPs) in a mitochondrion (M) and in the cytoplasm (**a**: A800;
725 **b**: A80); **c**, **d**) anatase NPs (arrows) adherent, crossing cell wall (CW) and in the intercellular
726 space (IS) (A800); **e**) portion of bulk treated root, the arrows indicate nuclei (B800); **f**) dense
727 large particles aggregate (arrow) in bulk treated cells (B800). CW, cell wall.
728
729
730
731
732
733
734
735

736

Table 1. Root growth and oxidative stress (hydrogen peroxide and thiobarbituric acid reactive substances, TBARS) in *Pisum sativum* plants grown for 28 days in farming soil (C1); in C1 amended with biosolid (C2) (**a**) and in the presence of 80 and 800 mg/Kg of TiO_2 nanoparticles (anatase, A; rutile, R; mix anatase+rutile 1:1 ratio) and bulk material, B (**b**). Data are reported as mean values ± SE. Means followed by the same letters within the same row are not significantly different at 5%.

a)

	C1	C2
Root Length (cm)	12.92±0.80a	10.69±0.33b
Hydrogen peroxide (μmol/gFW)	1.07±0.06a	0.97±0.07a
Lipid peroxidation (nanomol/gFW)	28.54±0.35a	28.87±0.86a

b)

	C2	R80	A80	Mix80	B80	R800	A800	Mix800	B800
Root Length (cm)	10.69±0.33a	8.82±0.57b	7.00±0.38c	8.10±0.42bc	7.71±0.58bc	8.60±0.52b	9.11±0.44b	9.18±0.55b	7.17±0.57c
Hydrogen peroxide (μmol/gFW)	0.97±0.07de	0.76±0.05ef	2.05±0.08a	1.47±0.08b	1.15±0.11cd	1.26±0.08bc	0.95±0.17def	0.68±0.08f	1.28±0.13bc
TBARS (nanomol/gFW)	28.87±0.86b	26.81±0.50cd	28.83±0.34b	28.68±0.20bc	26.14±0.13d	25.28±0.22d	25.93±0.46d	31.82±0.70a	26.14±0.19d

737

738

739

740

741

742

743

744

745

746

747

748

749

750

751

752

753

754 Figure 1

755

756

757

758

759

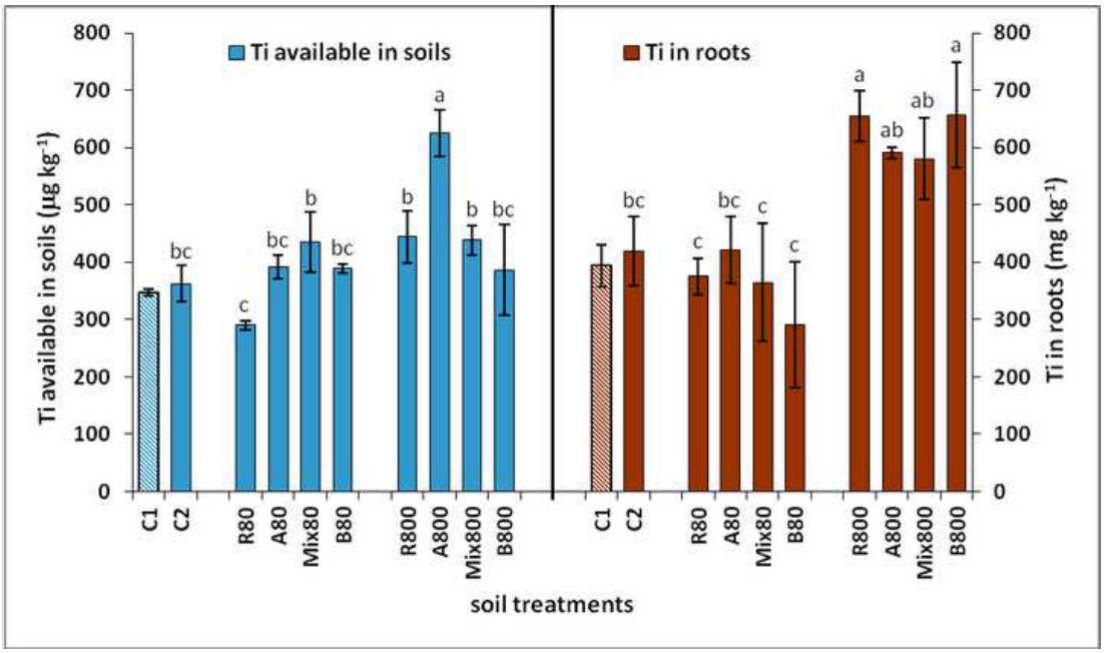

760

761

762

763

764

765

766

767

768

769

770 Figure 2

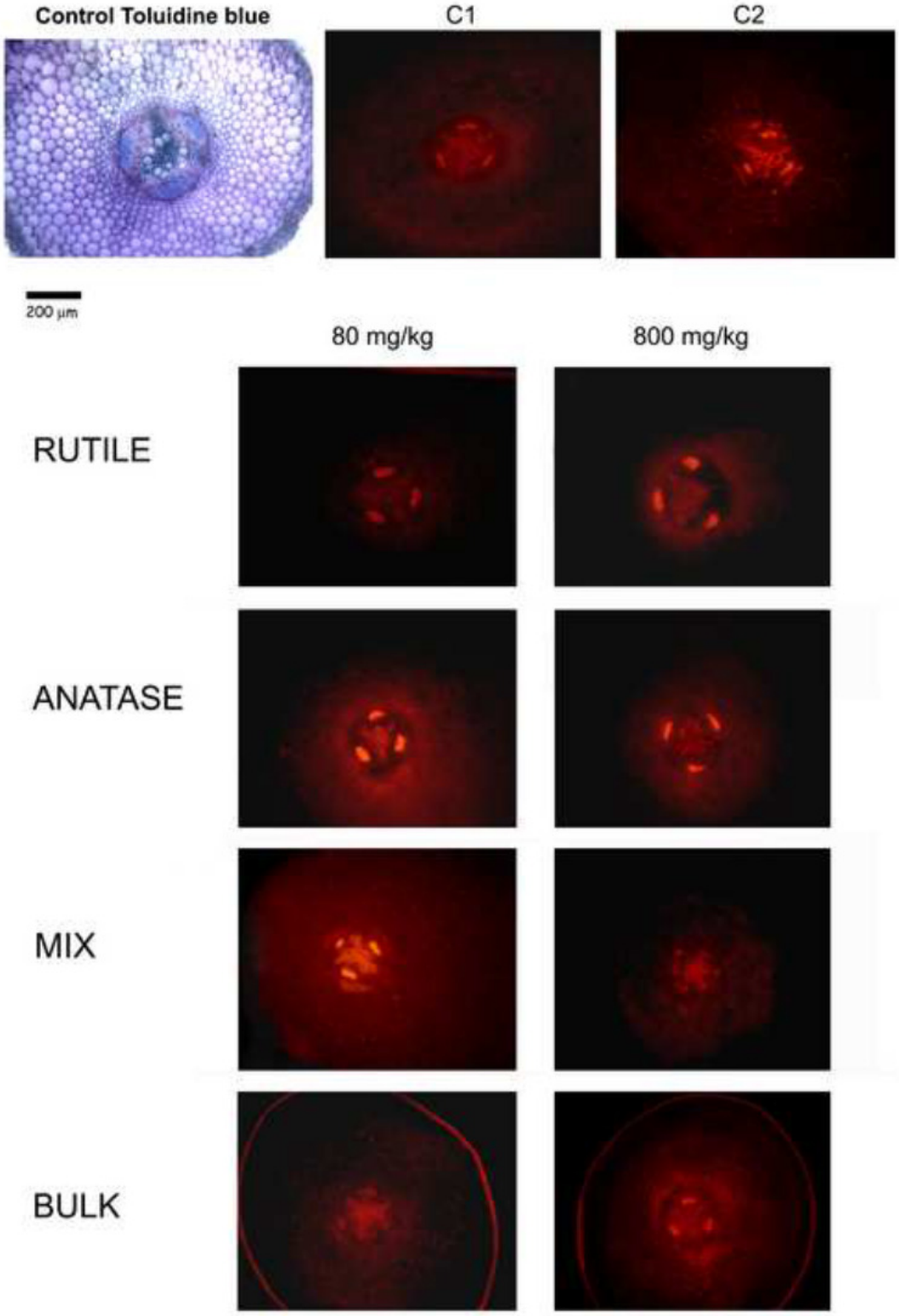

771

772

773 Figure 3

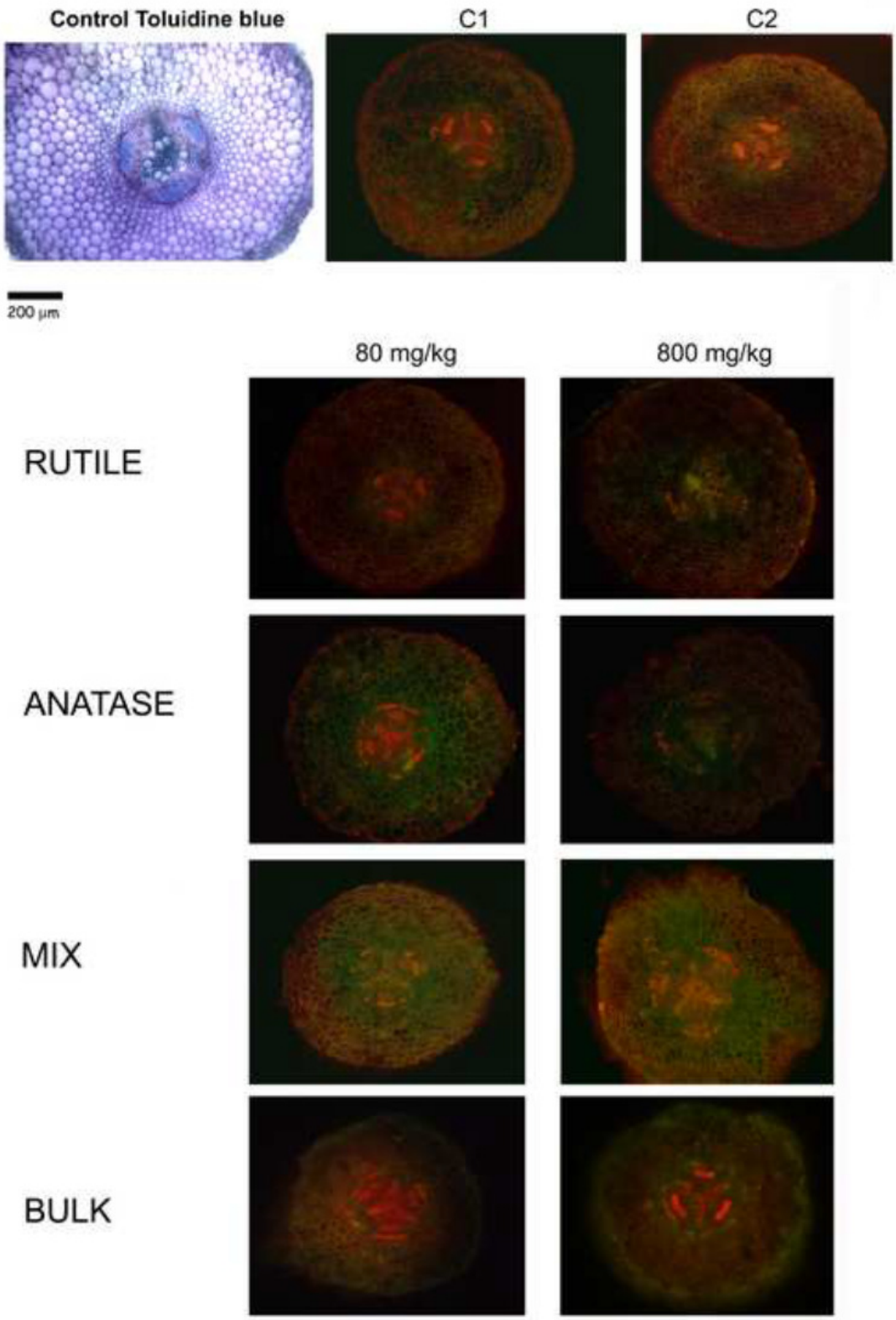

774

775

776 Figure 4

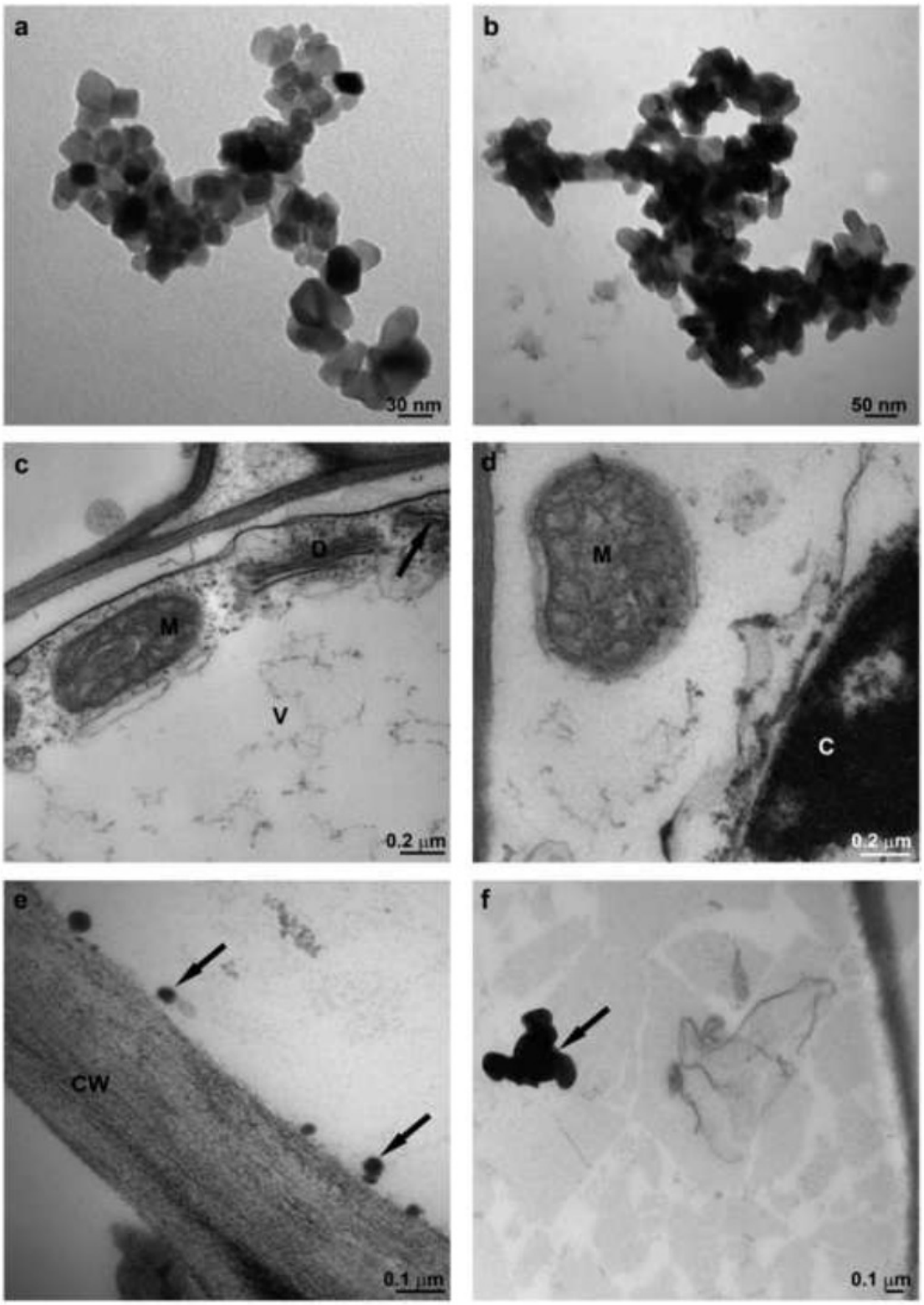

777

778

Figure 5

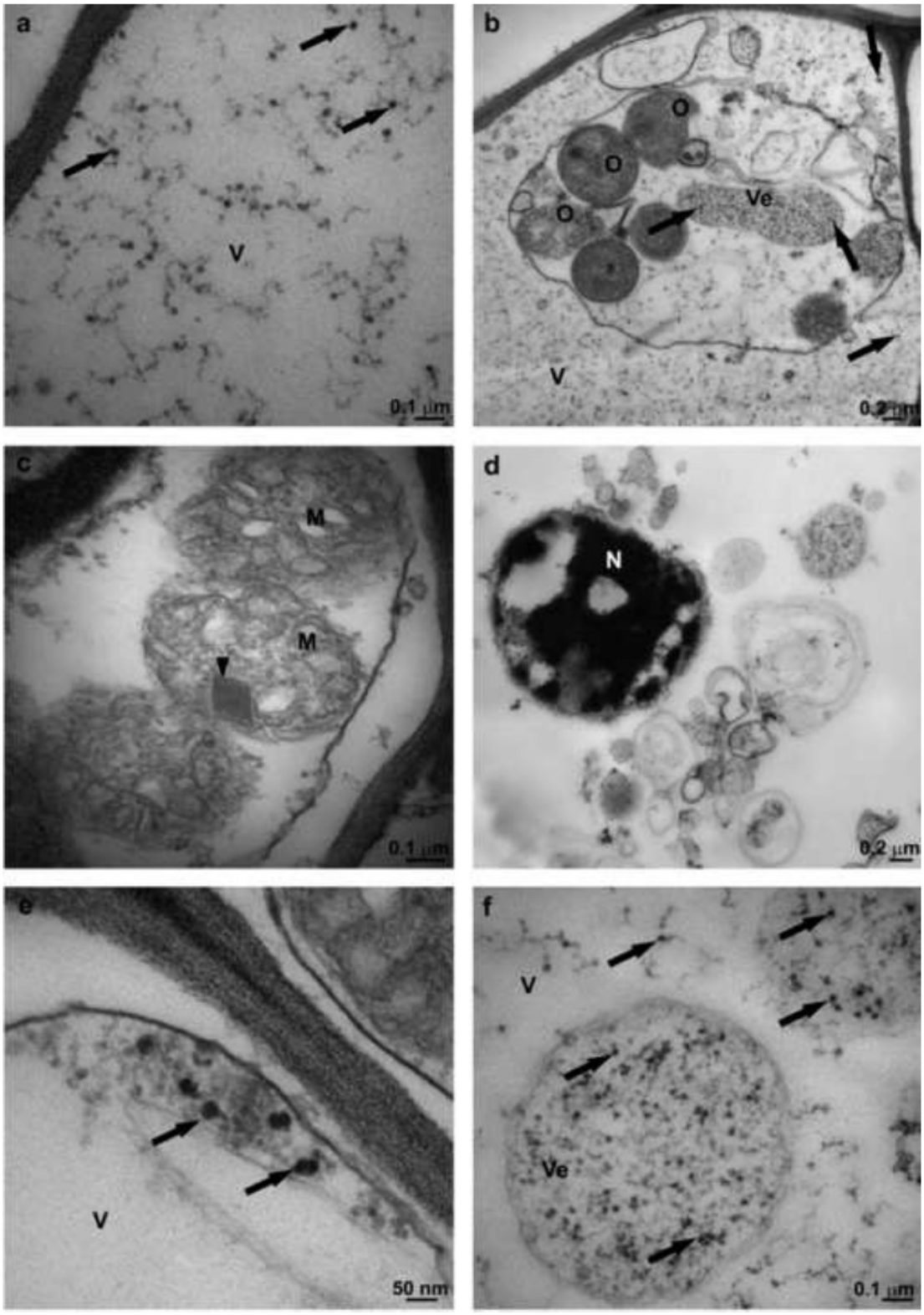

782 Figure 6

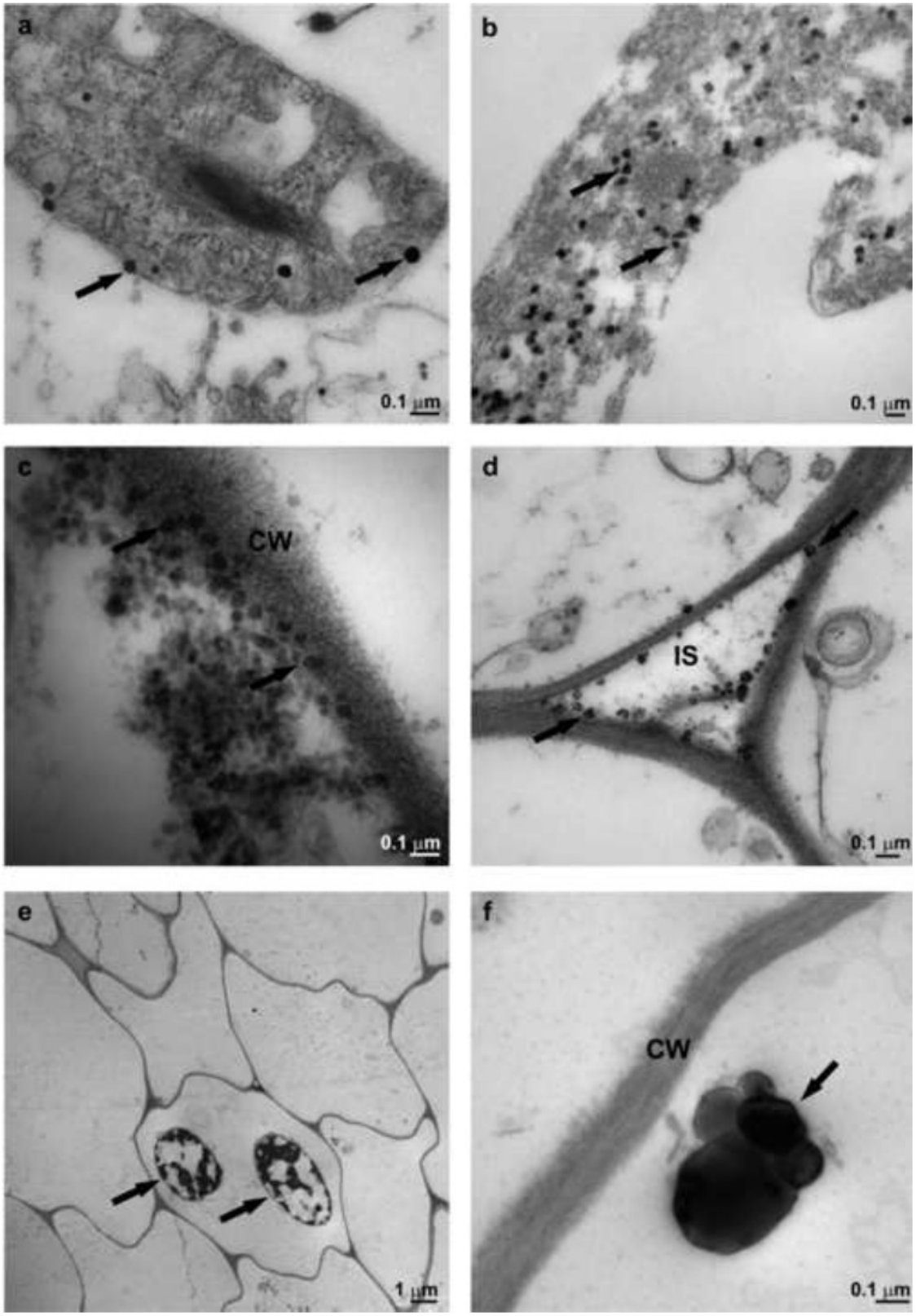

783